Applied Science and Engineering Progress, Vol. 12, No. 3, pp. 150–157, 2019

Research Article

A Comparison of the Roe's FDS, HLLC, AUFS, and AUSMDV$^+$ Schemes on Triangular Grids

Sutthisak Phongthanapanich*
Department of Mechanical Engineering Technology, College of Industrial Technology, King Mongkut's University of Technology North Bangkok, Bangkok, Thailand

Kazuyoshi Takayama
Tohoku University, Sendai, Japan

* Corresponding author. E-mail: sutthisak.p@cit.kmutnb.ac.th DOI: 10.14416/j.asep.2019.07.003
Received: 19 April 2019; Revised: -; Accepted: 17 June 2019; Published online: 9 July 2019

Abstract
The upwind schemes had proved to be effective for solving a wide variety of high-speed compressible flow problems due to their accuracy and robustness concerning other schemes. The unstructured grids had been commonly used to discretize the complex geometry then it is necessary to evaluate the performance of the upwind schemes on unstructured grids. This paper presents a comparison study of the accuracy and numerical stability of the Roe's FDS (RoeVLPA), HLLC, AUFS, and AUSMDV$^+$ schemes on two-dimensional triangular grids. It is found that the AUSMDV$^+$ scheme provides the most accurate solution and the AUFS scheme is the most dissipative scheme.

Keywords: AUFS, AUSMDV$^+$, HLLC, Roe's FDS, Triangular Grids

1 Introduction

The shock capturing finite-volume methods are commonly used to predict shocks in various aerodynamic flow situations with considerable success. The calculations of numerical fluxes across cell interfaces have become an essential research topic. The numerical scheme relies on an approximate Riemann solver must have the ability to predict discontinuities, strong shocks, and the propagating waves velocity accurately. However, many pieces of evidence can be concluded that most shock capturing methods fall short in predicting very strong shocks [1]–[7]. Roe's flux difference splitting (Roe's FDS) scheme [8] is known to possess good accuracy but to suffer from the numerical shock instability so-called the carbuncle phenomenon, violates entropy condition, and lacks positivity property. The method has some weakness and may fail or produce physically unrealistic numerical solutions for some problems including the high Mach number flow past a blunt body, the kinked Mach stem, and the moving shock in a straight duct from an odd-even grid perturbation. Many researchers [3]–[5] proposed the entropy fix methods to heal such numerical instabilities. It is found that the RoeVLPA scheme is a very accurate and robust scheme over a wide variety of high-speed compressible flow problems.

The HLL Riemann solver has proved extremely reliable and robust [9]. The simplest HLL approximation assumes only one intermediate wave state between the two acoustic waves. The main drawback is that it cannot resolve contact discontinuities exactly. The inability of the HLL scheme to resolve contact and shear waves was alleviated through the development

Please cite this article as: S. Phongthanapanich and K. Takayama, "A comparison of the Roe's FDS, HLLC, AUFS, and AUSMDV$^+$ schemes on triangular grids," *Applied Science and Engineering Progress*, vol. 12, no. 3, pp. 150–157, Jul.–Sep. 2019.

of the HLLC (Harten, Lax, Van-Leer, Contact) scheme [10], [11] by adding a contact wave to the pre-existing two-wave HLL structure. Then it has been widely used in CFD due to its ability for capturing shock, rarefaction, and contact discontinuity accurately. However, the scheme may produce the numerical shock instability that often occurs near the shock for multidimensional problems [1], [5].

The AUFS scheme [12] was proposed to split the flux vector of the Euler equations by introducing two artificial wave speeds. The direction of wave propagation is adjusted by these two wave speeds. If they are set to be the fastest wave speeds in two opposite directions, the method leads to the HLL approximate Riemann solver. The scheme is simple and can resolve sonic points smoothly. Moreover, the scheme can resolve exactly 1D stationary contact discontinuities. The robustness of the scheme is comparable with the exact Riemann solver.

The AUSM scheme [13] was presented as a simple, accurate, and robust method in comparison with existing numerical schemes and have become a very popular solution method. The scheme is developed by combining the accuracy of the FDS and the robustness of the flux-vector splitting scheme (FVS). Accuracy was improved especially on the boundary or in the shear layers. The attractive features of the AUSM scheme are 1) it does not require any characteristic analysis, 2) the ability to capture contact discontinuities exactly, and 3) require less computational time than many approximate Riemann solvers. Several attempts have been made in the following years to improve the original AUSM scheme. It is found that various AUSM-family schemes [14]–[16] can increase accuracy by reducing numerical diffusion and robustness for solving strong shock problems. Recently, the author proposes the AUSMDV$^+$ scheme [17] by combining the highly accurate AUSMD$^+$ scheme with the diffusive AUSMV$^+$ scheme, and the shock-capturing switch is redefined to identify the shock region effectively. Many test cases presented to confirm that the AUSMDV$^+$ scheme can solve a wide range of high-speed compressible flow problems accurately without shock anomalies, especially where strong physical discontinuities exist.

The objective of this work is to compare the numerical efficiency of the RoeVLPA, HLLC, AUFS, and AUSMDV$^+$ schemes on structured triangular grids. The paper is organized as follows. In Section 2, the governing equations and numerical flux formulations are presented. Then, the schemes are examined by benchmark test cases to evaluate their accuracy and robustness in Section 3.

2 The Numerical Scheme

2.1 *The governing equation and finite volume method*

The compact form of the two-dimensional Euler equations is

$$\mathbf{Q}_t + \nabla \cdot \mathbf{F} = \mathbf{0} \tag{1}$$

where $\mathbf{F} = \mathbf{E}\vec{i} + \mathbf{G}\vec{j}$ and [Equation (2)]

$$\mathbf{Q} = \begin{Bmatrix} \rho \\ \rho u \\ \rho v \\ \rho E \end{Bmatrix}, \mathbf{E} = \begin{Bmatrix} \rho u \\ \rho u^2 + p \\ \rho uv \\ \rho uH \end{Bmatrix}, \mathbf{G} = \begin{Bmatrix} \rho v \\ \rho uv \\ \rho v^2 + p \\ \rho vH \end{Bmatrix} \tag{2}$$

where ρ, u, v, p, E, and H denote density, x-velocity, y-velocity, pressure, total energy, and total enthalpy, respectively. The equation of state for a calorically perfect gas with a specific heat ratio $\gamma = 1.4$ is given by [Equation (3)]

$$p = \rho(\gamma - 1)\left[E - \frac{1}{2}\left(u^2 + v^2\right) \right] \tag{3}$$

By integrating Equation (1) over a control volume, Ω, and applying the divergence theorem to the resulting flux integral

$$\frac{\partial}{\partial t}\int_{\Omega} \mathbf{Q} d\Omega + \int_{\partial\Omega} \mathbf{F} \cdot \hat{\mathbf{n}} dS = 0 \tag{4}$$

where $\mathbf{F}$ is the numerical flux vector and $\hat{\mathbf{n}}$ is the normal unit vector to the cell boundary. By applying explicit Euler temporal integration to the first term of Equation (4), the second term is approximated by the sum of the fluxes crossing the faces of the control volume to yield [Equation (5)]

$$\Delta\mathbf{Q}_i + \frac{\Delta t}{\Omega_i}\left(\sum_{k=1}^{3} \mathbf{F}_k \cdot \hat{\mathbf{n}}_k S_k \right)_i = 0 \tag{5}$$

where S_k is the interface area and $\hat{\mathbf{n}}_k$ is the unit normal vector outward from the interface.

2.2 *RoeVLPA scheme*

The numerical flux vector at the cell interface between the left cell L and the right cell R of the RoeVLPA scheme [5] is written as [Equation (6)]

$$\mathbf{F}_n^{\text{RoeVLPA}} = \frac{1}{2}(\mathbf{F}_{nL} + \mathbf{F}_{nR}) - \frac{1}{2}\sum_{k=1}^{4} \alpha_k |\lambda_k| \mathbf{r}_k \tag{6}$$

where $\lambda_k = \lfloor V_n - a \quad V_n \quad V_n \quad V_n + a \rfloor^T$, α_k is the wave strength of the k^{th} wave, $\mathbf{r}_k$ is the corresponding right eigenvector, V_n is the normal velocity, and a is the speed of sound at the cell interface. These eigenvalues λ_k are modified by applying the entropy fixed method to enhance the robustness of the scheme and can be written as [Equation (7)]

$$|\lambda_k| = \begin{cases} |\lambda_{1,4}| & , |\lambda_{1,4}| \geq 2\eta^{VL} \\ \dfrac{|\lambda_{1,4}|^2}{4\eta^{VL}} + \eta^{VL} & , |\lambda_{1,4}| < 2\eta^{VL} \\ \kappa \max\left(|\lambda_{2,3}|, \eta^{PA} \right) & \end{cases} \tag{7}$$

where [Equations (8) and (9)]

$$\eta^{VL} = \max\left(\lambda_R - \lambda_L, 0 \right) \tag{8}$$

$$\eta^{PA} = \max(\eta_2, \eta_3, \eta_4, \eta_5) \tag{9}$$

The constant value κ is usually less than or equal to one for the first-order scheme.

2.3 *HLLC scheme*

The HLLC scheme is an improved version of the HLL scheme by restoring the contact surface. The numerical flux vector at the cell interface between the left cell L and the right cell R of the HLLC scheme [10], [11] is written as [Equation (10)]

$$\mathbf{F}_n^{\text{HLLC}} = \begin{cases} \mathbf{F}_L & 0 \leq S_L \\ \mathbf{F}_{*L} = \mathbf{F}_L + S_L(\mathbf{Q}_{*L} - \mathbf{Q}_L) & S_L < 0 < S_* \\ \mathbf{F}_{*R} = \mathbf{F}_R + S_R(\mathbf{Q}_{*R} - \mathbf{Q}_R) & S_* < 0 < S_R \\ \mathbf{F}_R & 0 \geq S_R \end{cases} \tag{10}$$

Where [Equations (11)–(14)]

$$S_* = \frac{\rho_R V_R (S_R - V_R) - \rho_L V_L (S_L - V_L) + p_L - p_R}{\rho_R (S_R - V_R) - \rho_L (S_L - V_L)} \tag{11}$$

$$\rho_{*\alpha} = \rho_\alpha \frac{S_\alpha - V_\alpha}{S_\alpha - S_*} \tag{12}$$

$$p_* = \rho_L (V_L - S_L)(V_L - S_*) + p_L \tag{13}$$

$$\rho_{*\alpha} = \rho_\alpha \frac{S_\alpha - V_\alpha}{S_\alpha - S_*} \tag{14}$$

and $\alpha = L, R$. We have to note that the contact wave speed, S_*, always gives $S_{*L} = p_{*R}$. The wave speeds are computed from [Equation (15)]

$$S_\alpha = \min(\tilde{V} - \tilde{c}, V_\alpha - c_\alpha) \tag{15}$$

where $\tilde{V}$ and $\tilde{c}$ are the Roe-averaged velocity and speed of sound quantities.

2.4 *AUFS scheme*

The convective flux of the AUFS scheme [12] is split into two parts as [Equation (16)]

$$\mathbf{F}_n^{\text{AUFS}} = (1 - \omega)\mathbf{F}_1 + \omega \mathbf{F}_2 \tag{16}$$

where [Equations (17)–(26)]

$$\mathbf{F}_1 = \frac{1}{2}(\mathbf{F}_{L\ pL}^{(\text{p})} + \mathbf{F}_R^{(\text{p})}) + \delta \mathbf{F}_u^{\text{AUFS}} \tag{17}$$

$$\mathbf{F}_2 = \begin{cases} (V_L - s_2)\mathbf{F}_L^{(\text{c})} + \mathbf{F}_L^{(\text{p})} & s_1 > 0 \\ (V_R - s_2)\mathbf{F}_R^{(\text{c})} + \mathbf{F}_R^{(\text{p})} & \text{otherwise} \end{cases} \tag{18}$$

$$\mathbf{F}_\alpha^{(\text{c})} = \begin{Bmatrix} \rho \\ \rho u \\ \rho v \\ \rho E \end{Bmatrix}_\alpha, \mathbf{F}_\alpha^{(\text{p})} = \begin{Bmatrix} 0 \\ p n_x \\ p n_y \\ pV \end{Bmatrix}_\alpha \tag{19}$$

$$\delta\mathbf{F}_u^{AUFS} = \frac{1}{2\bar{c}}\begin{pmatrix} p_L - p_R \\ (pu)_L - (pu)_R \\ (pv)_L - (pv)_R \\ \dfrac{\bar{c}^2\left(p_L - p_R\right)}{\gamma - 1} + \dfrac{1}{2}\left[(pV^2)_L - (pV^2)_R\right] \end{pmatrix} \quad (20)$$

$$\bar{c} = \frac{1}{2}(c_L + c_R) \quad (21)$$

$$s_1 = \frac{1}{2}(V_L + V_R) \quad (22)$$

$$s_2 = \begin{cases} \min(0, V_L - c_L, V_* - c_*) & \text{if } s_1 > 0 \\ \max(0, V_R + c_R, V_* + c_*) & \text{if } s_1 \le 0 \end{cases} \quad (23)$$

$$V_\alpha = \mathbf{u}_\alpha \cdot \hat{\mathbf{n}} \quad (24)$$

$$V_* = \frac{1}{2}(V_L + V_R) + \frac{(c_L - c_R)}{\gamma - 1} \quad (25)$$

$$c_* = \frac{1}{2}(c_L + c_R) + \frac{(\gamma - 1)(V_L - V_R)}{4} \quad (26)$$

and $\alpha = L, R$.

2.5 *AUSMDV+ scheme*

The AUSMDV$^+$ scheme is the application of hybrid strategies based on existing numerical methods may combine some advantages of different upwind schemes for improving the accuracy and stability of numerical computations. It is obtained by blending the AUSMD$^+$ and AUSMV$^+$ schemes [18]. The AUSMV$^+$ scheme is very stable but too diffusive, while the AUSMD$^+$ scheme is highly accurate but marginally stable. To take advantage of its efficient shock-capturing capability, the AUSMDV$^+$ scheme is a bias-averaging scheme toward the AUSMD$^+$ scheme, as follows

AUSMD$^+$: For all AUSM-family schemes, the inviscid flux is explicitly split into convective and pressure fluxes as [Equation (27)]

$$\mathbf{F}_n^{\text{AUSM}} = \mathbf{F}_n^{(c)} + \mathbf{F}_n^{(p)} \quad (27)$$

The numerical flux at the cell interface between the states $\mathbf{Q}_L$ and $\mathbf{Q}_R$ is given as [Equation (28)]

$$\mathbf{F}_n^{\text{AUSMD}^+} = \frac{1}{2}\Big[C_{1/2}(\boldsymbol{\Psi}_L + \boldsymbol{\Psi}_R) - \left|C_{1/2}\right|(\boldsymbol{\Psi}_R - \boldsymbol{\Psi}_L)\Big] + \mathbf{P}_{1/2} \quad (28)$$

Where [Equation (29)]

$$\boldsymbol{\Psi}_\alpha = \begin{Bmatrix} \rho \\ \rho u \\ \rho v \\ \rho H \end{Bmatrix}_\alpha, \mathbf{P}_{1/2} = \begin{Bmatrix} 0 \\ p_{1/2} n_x \\ p_{1/2} n_y \\ 0 \end{Bmatrix} \quad (29)$$

The common velocity $C_{1/2}$ is expressed as [Equation (30)]

$$C_{1/2} = c_{1/2}(C_L^+ + C_R^-) \quad (30)$$

The calculation of the interface speed of sound $C_{1/2}$, C_L^+, and C_R^- are available in Ref. [18]. The new pressure flux of Kitamura and Shima [17] is implemented into the scheme.

AUSMV$^+$: To construct the improved low-diffusion flux-vector splitting scheme, a numerical flux that explicitly expresses the mass flux at the cell interface can be written in a general form [19] as [Equations (31)–(34)]

$$\mathbf{F}_n^{\text{AUSMV}^+} = \frac{1}{2}\Big[m_{1/2}(\boldsymbol{\Psi}_L + \boldsymbol{\Psi}_R) - D_{1/2}(\boldsymbol{\Psi}_R - \boldsymbol{\Psi}_L)\Big] + \mathbf{P}_{1/2} \quad (31)$$

where

$$\boldsymbol{\Psi}_\alpha = \begin{Bmatrix} 1 \\ u \\ v \\ H \end{Bmatrix}_\alpha \quad (32)$$

$$m_{1/2} = m_{1/2}^+ + m_{1/2}^- \quad (33)$$

$$D_{1/2} = m_{1/2}^+ - m_{1/2}^- \quad (34)$$

AUSMDV$^+$: To take advantage of its efficient shock-capturing capability, the AUSMDV$^+$ scheme is a bias-averaging scheme toward the AUSMD$^+$ scheme as follows [Equation (35)]

$$\mathbf{F}_n^{\text{AUSMDV}^+} = \frac{1}{2}\left[(1+s)\mathbf{F}_n^{\text{AUSMV}^+} + (1-s)\mathbf{F}_n^{\text{AUSMD}^+}\right] \quad (35)$$

where s is defined by [Equation (36)]

$$s = 2\min\left(1.0, K\frac{|p_R - p_L|}{\max(\rho_L, \rho_R)}\right) - 1 \quad (36)$$

Following several numerical experiments, a constant parameter $K = 5$ is taken.

3 Test Problems and Discussion

In order to illustrate the accuracy and robustness of three numerical scheme, they must be evaluated via the first-order accuracy to limit the effects of the complexity of higher-order accuracy implementation. The above three schemes have been evaluated using three test cases. The selected test cases are 1) the Sod shock tube, 2) the Toro strong shock wave, and 3) the double Mach reflection of a strong shock.

3.1 *Sod shock tube*

The Sod shock tube problem [18], [20] is a common test case for the accuracy of numerical schemes. The solution of this problem can be described by solving the Euler equations which leads to three characteristics namely the shock wave, the contact discontinuity, and the rarefaction wave. The initial conditions for the left and right sides of an ideal gas are given by $(\rho, u, p)_L = (1.0, 0.0, 1.0)$ and $(\rho, u, p)_R = (0.125, 0.0, 0.1)$. The 1×0.1 computational domain is discretized with uniform triangular elements into 400 and 40 equal intervals in the x and y directions, respectively.

Figures 1 shows the predicted density and distributions along the tube length and is compared with the exact solutions at a time t = 0.15. All schemes provide non-oscillate solutions. The zoom in of the shock wave, the contact discontinuity, and the rarefaction wave are depicted in Figure 2(a)–(c), respectively. It is seen that the accuracy of all schemes to capture shock wave and contact discontinuity are not significantly different as shown in Figure 2(a)–(b). Moreover, the AUSMDV$^+$ scheme gives the most accurate solution and very close to the exact solution as shown in Figure 3(c).

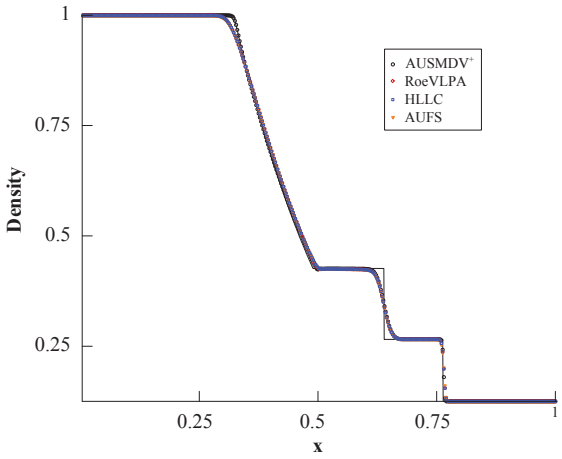

Figure 1: Comparison of numerical and exact solutions at time t = 0.15 for problem 3.1.

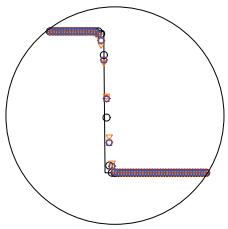

(a) Shock wave

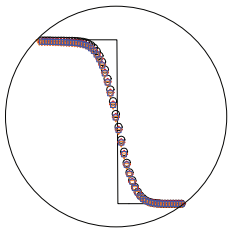

(b) Contact discontinuity

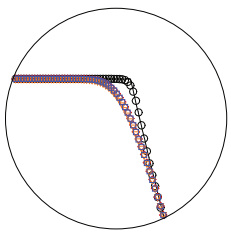

(c) Rarefaction wave

Figure 2: Zoom in on Figure 1.

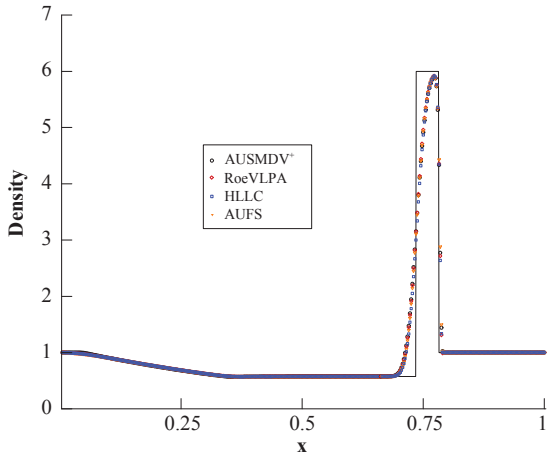

Figure 3: Comparison of numerical and exact solutions at time $t = 0.012$ for problem 3.2.

3.2 *Toro strong shock wave*

The initial conditions of this shock tube problem are given by $(\rho, u, p)_L = (0.1, 0.0, 1000.0)$ and $(\rho, u, p)_R = (0.1, 0.0, 0.1)$ [5], [21]. The difficulty of this problem is that the shock and the contact discontinuity are very close to each other. It is thus very difficult for most of the numerical schemes to capture both the shock and the contact discontinuity within such a few elements. The same computational domain as described in problem 3.1 is used again. Figure 3 shows the predicted density and distributions along the tube length and are compared with the exact solutions at a time $t = 0.012$. There is no difference in the numerical solutions obtained from these four schemes. Figure 4(a)–(c) illustrated that four schemes provide a very similar solution; however, the AUSMDV$^+$ scheme gives better expansion wave solution than the RoeVLPA, HLLC, and AUFS schemes.

3.3 *Mach 2 reflection over a 46° wedge*

The last problem is a Mach number 2 shock is reflected from a 46° wedge [5]. The wave configuration and an interferogram as obtained in shock tube experiment are shown in Figure 5. The computational domain is discretized by the structured triangular grids ($\Delta x = \Delta y = 1/250$). Figures 6 to 9 show the density contours at the time $t = 0.7$ ms of the AUSMDV$^+$, RoeVLPA, HLLC, and AUFS schemes,

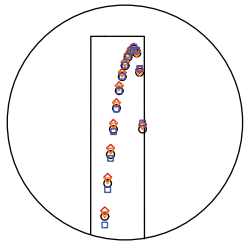

(a) Shock wave

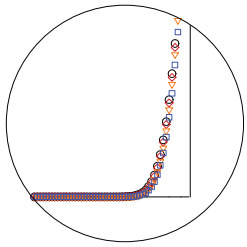

(b) Contact discontinuity

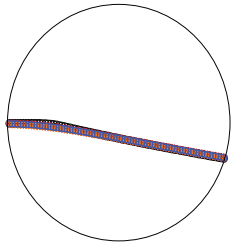

(c) Rarefaction wave

Figure 4: Zoom in on Figure 3.

Figure 5: Interferogram of the Mach 2 reflection over a 46° wedge: $Ms = 2$ in the air at $T = 298.65$ K and $p_0 = 250$ hPa (courtesy of K. Takayama).

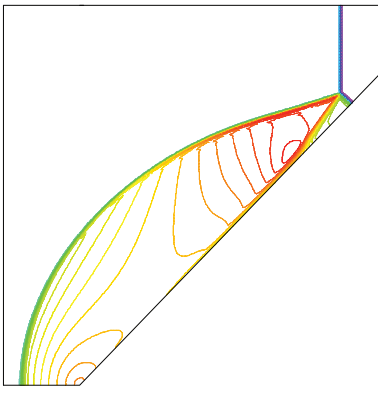

Figure 6: Density control of the problem 3.3: AUSMDV^{+}.

Figure 7: Density control of the problem 3.3: RoeVLPA.

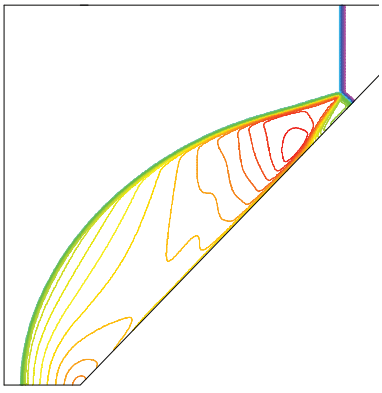

Figure 8: Density control of the problem 3.3: HLLC.

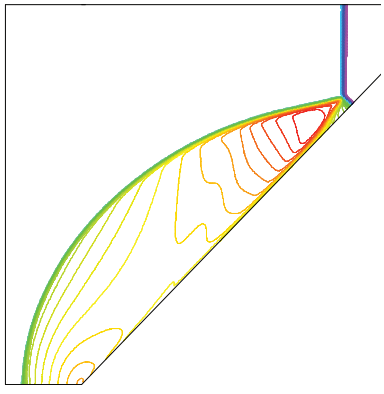

Figure 9: Density control of the problem 3.3: AUFS.

respectively. The results presented that all schemes provided a stable solution and similar to an experiment data given by Figure 5. By considering at the triple point and the length of the Mach stem, the AUSMDV^{+} scheme gives the most accurate solution. The RoeVLPA and HLLC schemes show a similar solution with slightly shorter Mach stem compared to the AUSMDV^{+} scheme. The AUFS scheme is the most dissipate scheme then it gave the shortest Mach stem.

4 Conclusions

The accuracy and robustness of the AUSMDV^{+}, RoeVLPA, HLLC, and AUFS schemes for solving two-dimensional high-speed compressible flow problems on structured triangular grids were investigated in this paper. The Sod shock tube and the Toro strong shock wave are chosen as the test cases because there are the exact solutions. It may be concluded that the AUSMDV^{+} scheme can capture an expansion wave accurately than other schemes. All schemes give a similar solution to the shock wave and the contact discontinuity. Finally, the Mach 2 reflection over a 46° wedge is selected to test the robustness against the carbuncle phenomenon and the accuracy of the schemes. The AUSMDV^{+} scheme provided the most accurate solution, the RoeVLPA and HLLC schemes reported a similar solution, and the AUFS scheme gave the most dissipate solution with the shortest length of the Mach stem.

Acknowledgments

The first author is grateful to the College of Industrial Technology, King Mongkut's University of Technology North Bangkok, Bangkok, Thailand for funding this research work.

References

[1] J. J. Quirk, "A contribution to the great Riemann solver debate," *International Journal for Numerical Methods in Fluids*, vol. 18, pp. 555–574, 1994.

[2] J. C. Robinet, J. Gressier, G. Casalis, and J. M. Moschetta, "Shock wave instability and the carbuncle phenomenon: Same intrinsic origin?," *Journal of Fluid Mechanics*, vol. 417, pp. 237–263, 2000.

[3] M. Pandolfi and D. D'Ambrosio, "Numerical instabilities in upwind methods: Analysis and cures for the "Carbuncle" phenomenon," *Journal of Computational Physics*, vol. 166, pp. 271–301, 2001.

[4] M. Dumbser, J. M. Moschetta, and J. Gressier, "A matrix stability analysis of the carbuncle phenomenon," *Journal of Computational Physics*, vol. 197, pp. 647–670, 2004.

[5] S. Phongthanapanich and P. Dechaumphai, "Healing of shock instability for Roe's flux-difference splitting scheme on triangular meshes," *International Journal for Numerical Methods in Fluids*, vol. 59, pp. 559–575, 2009.

[6] M. V. C. Ramalho, J. H. A. Azevedo, and J. L. F. Azevedo, "Further investigation into the origin of the carbuncle phenomenon in aerodynamic simulations," presented at the 49th AIAA Aerospace Sciences Meeting including the New Horizons Forum and Aerospace Exposition, Florida, US, Jan. 4–7, 2011.

[7] S. Phongthanapanich, "Healing of the carbuncle phenomenon for AUSMDV scheme on triangular grids," *International Journal of Nonlinear Sciences and Numerical Simulation*, vol. 17, pp. 15–28, 2016.

[8] P. L. Roe, "Approximate Riemann solvers, parameter vectors, and difference schemes," *Journal of Computational Physics*, vol. 43, pp. 357–372, 1981.

[9] A. Harten, P. D. Lax, and B. Van Leer, "On upstream differencing and Godunov-type schemes for hyperbolic conservation laws," *SIAM Review*, vol. 25, pp. 35–61, 1983.

[10] E. F. Toro, M. Spruce, and W. Speares, "Restoration of the contact surface in the HLL-Riemann solver," *Shock Waves*, vol. 4, pp. 25–34, 1994.

[11] P. Batten, N. Clarke, C. Lambert, and D. M. Causon, "On the choice of waves speeds for the HLLC Riemann solver," *SIAM Journal on Scientific Computing (SISC)*, vol. 18, pp. 1553–1570, 1997.

[12] M. Sun and K. Takayama, "An artificial upstream flux vector splitting scheme for the Euler equations," *Journal of Computational Physics*, vol. 189, pp. 305–329, 2003.

[13] M. S. Liou and C. J. Steffen, "A new flux splitting scheme," *Journal of Computational Physics*, vol. 107, pp. 23–39, 1993.

[14] M. S. Liou, "A sequel to AUSM: AUSM$^+$," *Journal of Computational Physics*, vol. 129, pp. 364–382, 1996.

[15] Y. Wada and M. S. Liou, "An accurate and robust flux splitting scheme for shock and contact discontinuities," *SIAM Journal on Scientific Computing (SISC)*, vol. 18, pp. 633–657, 1997.

[16] K. H. Kim, C. Kim, and O. H. Rho, "Methods for the accurate computations of hypersonic flows I. AUSMPW$^+$ scheme," *Journal of Computational Physics*, vol. 174, pp. 38–80, 2001.

[17] K. Kitamura and E. Shima, "Towards shock-stable and accurate hypersonic heating computations: A new pressure flux for AUSM-family schemes," *Journal of Computational Physics*, vol. 245, pp. 62–83, 2013.

[18] S. Phongthanapanich, "An accurate and robust AUSM-family scheme on two-dimensional triangular grids," *Shock Waves*, vol. 29, no. 5, pp. 755–768, 2019.

[19] S. Phongthanapanich, "A parameter-free AUSM-based scheme for healing carbuncle phenomenon," *Journal of the Brazilian Society of Mechanical Sciences and Engineering*, vol. 38, pp. 691–701, 2016.

[20] G. A. Sod, "A survey of several finite difference methods for systems of nonlinear hyperbolic conservation laws," *Journal of Computational Physics*, vol. 27, pp. 1–31, 1978.

[21] E. F. Toro, *Riemann Solvers and Numerical Methods for Fluid Dynamics*. Berlin, Germany: Springer, 1999.